A&A 496, 713–724 (2009)
DOI: 10.1051/0004-6361/200811175

Astronomy & Astrophysics

Spectral and intensity variations of Galactic ^{26}Al emission

W. Wang[1,2], M. G. Lang[1], R. Diehl[1], H. Halloin[3], P. Jean[4], J. Knödlseder[4], K. Kretschmer[1], P. Martin[4], J. P. Roques[4], A. W. Strong[1], C. Winkler[5], and X. L. Zhang[1]

[1] Max-Planck-Institut für extraterrestrische Physik, Postfach 1312, 85741 Garching, Germany
e-mail: wwang@mpe.mpg.de
[2] National Astronomical Observatories, Chinese Academy of Sciences, Beijing 100012, PR China
[3] AstroParticule et Cosmologie (APC), 11 place Marcelin Berthelot, 75231 Paris, France
[4] Centre d'Étude Spatiale des Rayonnements, BP 4346, 31028 Toulouse Cedex 4, France
[5] ESA-ESTEC, Keplerlaan 1, 2201 AZ Noordwijk, The Netherlands

Received 17 October 2008 / Accepted 28 January 2009

ABSTRACT

Aims. Gamma-ray line emission from the radioactive decay of ^{26}Al reflects nucleosynthesis in massive stars and supernovae. We use INTEGRAL ^{26}Al measurements to characterize the distribution and characteristics of ^{26}Al source regions throughout the Galaxy.
Methods. The spectrometer SPI aboard INTEGRAL has accumulated over five years of data on ^{26}Al gamma-ray emission from the Galactic plane. We analyzed these data using suitable instrumental-background models and adopted sky distribution models to produce high-resolution ^{26}Al spectra of Galactic emission, spatially resolved along the Galaxy plane.
Results. We detect the ^{26}Al line from the inner Galaxy at $\sim 28\sigma$ significance. The line appears narrow, and we constrain broadening in the source regions to <1.3 keV (2σ). Different sky distribution models do not significantly affect those large-scale results. The ^{26}Al intensity for the inner Galaxy is derived as $(2.9 \pm 0.2) \times 10^{-4}$ ph cm^{-2} s^{-1} rad^{-1}, consistent with earlier results from COMPTEL and SPI data. This can be translated to an ^{26}Al mass of $2.7 \pm 0.7\ M_{\odot}$ in the Galaxy as a whole. The ^{26}Al intensity is also confirmed to be somewhat brighter in the 4th than in the 1st quadrant (ratio $\sim 1.3 \pm 0.2$). ^{26}Al spectra separately derived for regions along the Galactic plane show clear line centroid shifts, attributed largely to the Galaxy's large-scale rotation. The ^{26}Al line toward the direction of the Aquila region ($20^{\circ} < l < 40^{\circ}$) appears somewhat broadened. Latitudinal variations of ^{26}Al emission towards the inner Galaxy are studied, finding a latitudinal scale height of 130^{+120}_{-70} pc (1σ) for ^{26}Al in the inner Galaxy and a hint (3σ) of peculiar ^{26}Al emission towards the region $l < 0^{\circ}$, $b > 5^{\circ}$.

Key words. Galaxy: abundances – ISM: abundances – nuclear reactions, nucleosynthesis, abundances – gamma rays: observations

1. Introduction

The unstable isotope ^{26}Al has a mean lifetime of 1.04 Myr. ^{26}Al first decays into an excited state of ^{26}Mg, which de-excites into the ^{26}Mg ground state by emitting gamma-ray photons with the characteristic energy of 1809 keV. The 1809 keV gamma-ray line from radioactive ^{26}Al serves as a tracer of the recent nucleosynthesis activity in the Galaxy.

The 1809 keV γ-ray line emission from the Galaxy was first detected with the Ge spectrometer on the HEAO-C space experiment (Mahoney et al. 1982). The Compton Observatory sky survey 1991−2000 then with COMPTEL imaging of the ^{26}Al line across the sky showed that ^{26}Al emission extends along the Galactic plane, thus clearly establishing ^{26}Al nucleosynthesis as a widely-distributed Galactic phenomenon (Diehl et al. 1995; Plüschke et al. 2001). The structure of this emission, alignments of emission maxima with spiral-arm tangent, and comparisons with tracers of candidate ^{26}Al sources, all point to a predominant origin of ^{26}Al in massive stars (Prantzos & Diehl 1996; Chen et al. 1995; Diehl et al. 1995; Knödlseder 1999).

The detailed study of ^{26}Al line emission from the Galaxy is one of the main science goals of the INTEGRAL mission. SPI aboard INTEGRAL is a high-resolution spectrometer with energy resolution of 3 keV (*FWHM*) at 1809 keV, which therefore adds high-resolution spectroscopic information to ^{26}Al astronomy. The Compton Observatory in its early design phase included a fifth instrument "GRSE", a high-resolution spectrometer later abandoned for cost and complexity reasons. COMPTEL as a scintillation-detector based instrument had modest spectral resolution of about 10% (*FWHM*). The detailed measurement of ^{26}Al line position and shape is expected to reveal more information beyond the COMPTEL imaging survey about the ^{26}Al sources and their location through the Doppler effect, induced from Galactic rotation and dynamics of the ejected ^{26}Al as it propagates in the interstellar medium around its stellar sources.

Earlier INTEGRAL analysis had used 1.5 years of SPI data to first explore the large-scale spectral characteristics of ^{26}Al emission in the inner Galaxy (Diehl et al. 2006a,b). A detection of the ^{26}Al line from the inner Galaxy with a significance of $\sim 16\sigma$ confirmed the narrowness of the ^{26}Al line (*FWHM* < 2.8 keV, 2σ), which had already been seen by RHESSI (Smith et al. 2003) and HEAO-C (Mahoney et al. 1984) earlier. We use INTEGRAL/SPI data accumulated from five years to extend this study towards spatially-resolved details of ^{26}Al line spectroscopy across the inner regions of the Galaxy. In this paper, we concentrate on the spectral and intensity variations of ^{26}Al emission along the Galactic plane. The main goal is to explore if there are variations from the large-scale properties of ^{26}Al emission, such as bulk motion or enhanced turbulence in specific regions. Our study will be limited by the brightness of the signal per region, and hence proceed from broad to more constrained regions

along the plane, as the current exposure and ^{26}Al brightness allows; with more exposure, in particular towards outer regions of the Galaxy at higher longitudes, the extended INTEGRAL mission is expected to eventually allow such studies up to the spatial resolution of about 2.8° (*FWHM*) of the SPI instrument. We also derive spectra for separate regions of Galactic latitudes, to probe the symmetry and the scale height of Galactic ^{26}Al emission.

In this paper, we first describe the SPI observations and methods of data analysis. Then we proceed with an update of the large-scale characteristics of Galactic ^{26}Al emission, before refining the spatial resolution of our study. We discuss the implications of our findings with respect to the large-scale distribution of ^{26}Al sources, the interstellar medium in their vicinity, and possible regional deviations. Studies of specific regions and their ^{26}Al emission are underway and will be reported in separate papers (Cygnus – Martin et al., in preparation; Orion – Lang et al., in preparation; Sco-Cen – Diehl et al., in preparation).

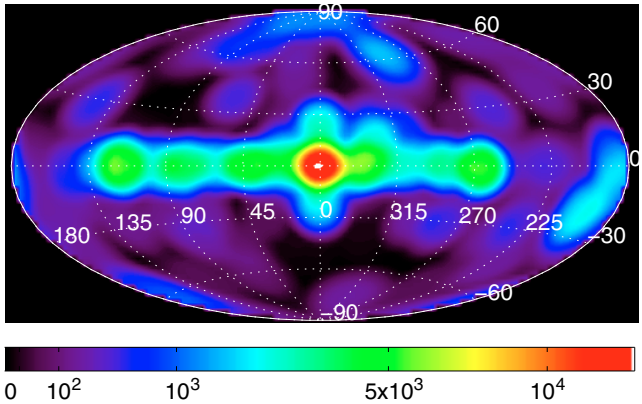

Fig. 1. Exposure of the sky in Galactic coordinates (the number at the color bar in units of ks) for the data selected from 5-year SPI observations for our ^{26}Al study (INTEGRAL orbits 43–650). The database covers the whole sky, with 29 736 individual pointings, equivalent to a total (deadtime-corrected) exposure time of 61 Ms. Observations emphasize the Galactic plane, specially in the inner Galaxy region, but also specific regions of interest such as Cas A, Cygnus, Carina-Vela, Orion, Virgo, and the Crab pulsar and nebula.

2. Observations and data analysis

2.1. SPI observations

The INTEGRAL spacecraft was launched on October 17, 2002, into a high-inclination, high-eccentricity orbit intended to avoid the increased background from the Earth's trapped radiation belts. INTEGRAL's orbital period is ~3 days. The spectrometer SPI consists of 19 Ge detectors actively shielded by a BGO anti-coincidence shield. It has a tungsten coded mask in its aperture which allows imaging at ~2.8° resolution within a 16° × 16° full coded field of view (imaging on INTEGRAL is mainly performed at lower energies by the IBIS telescope, with which SPI is co-aligned). The Ge detectors are sensitive to gamma-rays between 15 keV and 8 MeV, with a total effective area ~70 cm^2 at 1 MeV, and achieve an energy resolution of ~2.5 keV at 1 MeV (Roques et al. 2003; Attié et al. 2003). However, cosmic-ray (CR) impacts degrade this resolution over time, and the instrument SPI is periodically switched off for 14 days twice a year while annealing (by heating from cryogenic temperatures ~80 K to 100 °C) is applied to the detectors to restore the energy resolution back to its pre-launch value by thermal curing heating of the CR-induced defects (Roques et al. 2003; Leleux et al. 2003).

In space operations, INTEGRAL with its IBIS and SPI telescopes is pointed with a fixed attitude for intervals of typically ~2000 s (referred to as *pointings*), which are successively arranged as a standard pattern of neighbouring pointings ≃2° apart (*dithering*), and covering target region of interest for improved imaging (Jensen et al. 2003; Courvoisier et al. 2003).

We obtain a database from the 5-year SPI observations, i.e. from the INTEGRAL orbits 43–650, which encompasses 29 736 pointings of the spacecraft and its instruments across the sky, equivalent to a total deadtime-corrected exposure time of 61 Ms (see the exposure map in Fig. 1).

The instrument operation has been interrupted from a few short anomalies and the occurrences of solar flares, and most significantly for the typically two-week annealing episodes described above, and by the regular perigee passages with switch-offs due to the high background intensity from the radiation belts. The sensitivity of our observations were further reduced by the failure of two of the 19 detectors (December 2003 and July 2004).

2.2. Data analysis

Our data analysis steps include: (1) selection and assembly of data which are free of contaminations by anomalies and, e.g., solar-flare events; (2) modelling the instrumental background; (3) deriving spectra by fitting the measured data in narrow energy bins with our background model and a model of the spatial distribution of celestial gamma-ray emission, folded through the instrumental response into the data space of the measurement. These steps have been described in several papers, e.g. Strong et al. (2005), Diehl et al. (2003), and as applied to gamma-ray lines specifically in Wang et al. (2007) and Diehl et al. (2006b). Here we give a concise summary and add comments as relevant for the studies of this paper.

We first apply a selection filter to reject corrupted or invalid data. This is done for data sections called "science window", typically a time interval of ~30 min corresponding to one pointing. We apply selection windows to "science housekeeping" parameters such as the count rates in several background tracers, proper instrument status codes, and orbit phase. For tracing background, we employ the SPI plastic scintillator anticoincidence counter (PSAC), and the rate of saturating events in SPI's Ge detectors (i.e., events depositing >8 MeV in a single Ge detector; hereafter referred to as GEDSAT rates, see Fig. 2). This leads to exclusions of solar-flare periods and other periods of clearly increased / abnormal backgrounds. Additionally, regular background increases during and after passages through the Earth's radiation belts are eliminated through a 0.05–0.916 window on orbital phase.

From the selected events, spectra are accumulated per each detector and pointing in energy bins of 0.5 keV in the spectral range of 1785–1826 keV, and together with dead time and pointing information assembled into the analysis database. From identically-selected data, we also establish a database for the background modelling from the adjacent continuum, combining broader spectral ranges on both sides of the ^{26}Al line into single bins.

We select events which trigger one and only one of our 19 Ge detectors ("single events", SE). We exclude the ≃50% fraction of "multiple" events, because for events interacting in

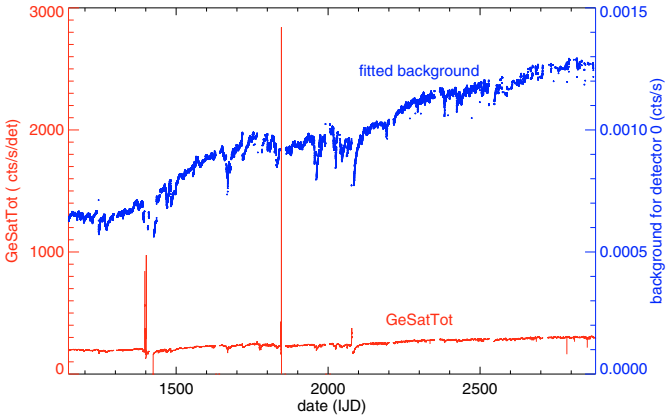

Fig. 2. The unfiltered total GEDSAT rates and background rates for detector 0 around 1809 keV in model fittings versus time (the INTEGRAL Julian Date, starts at 1 Jan. 2000). The total GEDSAT rates per detector generally vary in a range from 150−300 counts/s, but some erratic cases like zero values and solar flare spikes are excluded from science analysis with our primary selections (also see the text).

more than one detector different combinations of single-detector energies with their correspondingly-different resolutions would be superimposed for identical values of total energy, thus leading to an ill-determined spectral energy response. This reduces the total signal obtained, but guarantees that the spectral response of the instrument is well-defined for our dataset.

Instrumental background is dominated by a rather smooth spectral continuum, with instrumental lines superimposed – for our case, a broad instrumental-line feature centered at 1810 keV comprises 30% of the count rate (see Fig. 2 in Diehl et al. 2006b). For our model of the continuum background, we make use of the simultaneously-measured events in energy bands adjacent to the ^{26}Al line region, at 1785−1802 keV plus 1815−1826 keV, and use each detector's count rates in this adjacent range to normalize the GEDSAT time series with their superior statistical precision at regular intervals of several days. In Fig. 2 we show both the original GEDSAT count rate history and the background model for one of our detectors, as it varies over the dataset. It is seen that anomalous spikes of our background are excluded from our data, and that there still is significant temporal structure in our fitted background model. This "adjacent-energies" background variation model per detector thus is based on high-statistics GEDSAT rates over short time scales of ∼100 pointings, as these have been found to trace the prompt CR activation rather well. Adjusting these "templates" to the actual counts per detector in the 0.5 keV bins used for spectral analysis of the sky signal then ensures that over longer time scales (typically 3 days, where counts in those narrow bins are statistically sufficient) any second-order deviations from GEDSAT tracing actual backgrounds are accounted for. Through this procedure we ensure that pointing-to-pointing variations are given by our background tracer, independent of the coded-mask orientation on the sky. The broad instrumental line feature centered at 1810 keV is actually found to also be rather well modelled by these 0.5 keV bin adjustments, indicating that the line and continuum backgrounds have similar temporal behaviour.

The cosmic-signal spectra are obtained from our measured database of detector spectra when we combine above background models with a spatial model for sky emission (Fig. 3), allowing for adjustments of intensity parameters for background and sky intensities per energy bin:

$$D_{e,d,p} = \sum_{m,n} \sum_{j=1}^{k_1} A^{j,m,n}_{e,d,p} \beta^j_s I^{m,n}_j + \sum_t \sum_{i=1}^{k_2} \beta^i_{b,t} B^i_{e,d,p} + \delta_{e,d,p}, \quad (1)$$

where *e, d, p* are indices for data space dimensions: energy, detector, pointing; *m, n* indices for the sky dimensions (galactic longitude, latitude); A is the instrument response matrix, I is the intensity per pixel on the sky, k_1 is the number of independent sky intensity distribution maps; k_2 is the number of background components, δ is the count residue after the fitting. The coefficients β_s for the sky map intensity are constant in time, while $\beta_{b,t}$ is allowed time dependent, to cater for different background normalizations for each camera configuration of 19/18/17 functional detector elements. The sky brightness amplitudes β_s comprise the resultant spectra of the signal from the sky. We generally use a maximum-likelihood fitting method (implemented in a SPI standard tool called *spimodfit*, properly accounting for Poisson statistics in our spectra; for more details, see Strong et al. 2005).

We thus obtain per energy bin the fitted intensity parameter values with their uncertainties, their covariance matrices, and the fit residuals. Analysis of residuals, uncertainties, and covariance matrices are made to determine the validity of the fit of such a combined model to our measured set of spectra. Residuals after the model fitting are shown in Fig. 4 (residuals with the time and energies). Reduced χ^2 values around 1.0 confirm that both our background model and the sky distribution model(s) are adequate.

We use the sky intensity distribution of ^{26}Al as derived from 9 years of COMPTEL observations (maximum entropy map, Plüschke et al. 2001) as the standard reference sky model. We compare this to different ^{26}Al emission tracer models or maps, to assess the impact of different sky distribution models on the ^{26}Al line shape and intensity (see Sect. 3). For simultaneous fits of sets of partial-sky distribution models (in order to derive spatially-resolved spectra), we use analytical forms of sky distribution models with prescribed symmetry to avoid biases to such analysis (see below).

After we obtain fitted-amplitude coefficient spectra for the sky components, we characterize these spectra and in particular the ^{26}Al line details therein through two different approaches. When the sky signal is weak, we fit the spectra with Gaussians plus a linear residual background, and use the Gaussian intensities, centroid energies, and *FWHM* widths for relative comparisons, such as trends along the plane of the Galaxy. When the signal is sufficiently strong so that we are sensitive to line width details, we describe the line component not by a single Gaussian any more, but rather by the convolution of a Gaussian with the asymmetric instrumental line response as it develops from degradation of our detectors' resolution and their periodic restorations through annealings. This allows us to infer immediate information about the celestial ^{26}Al dynamics, which we identify with this Gaussian, and in particular its width, which arises from Doppler shifting of the line energies with motion of decaying ^{26}Al nuclei relative to the observer. In both cases, we fit these spectral models to the amplitude values and their uncertainties as determined from the model fit to the large set of spectra, performing a maximum-likelihood fit with the Levenberg-Marquardt algorithm. In the latter case, we derive the entire probability distribution of the fitted parameter values through a Monte Carlo Markov Chain (MCMC) method, which allows us

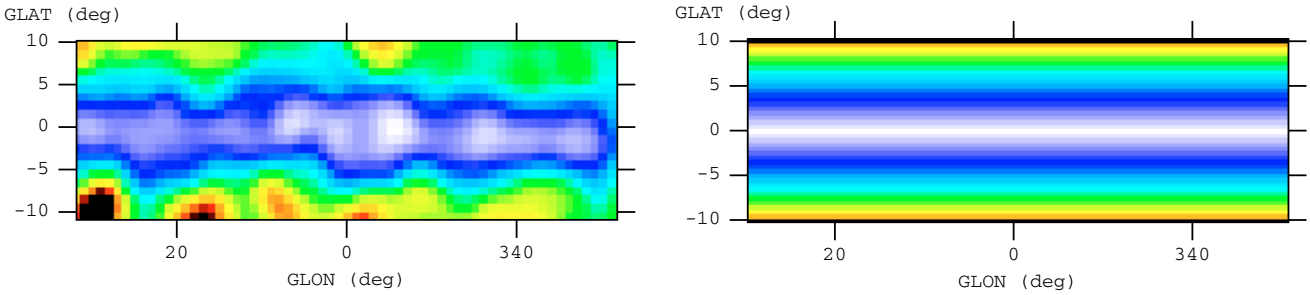

Fig. 3. The COMPTEL maximum entropy ^{26}Al map (*left*, Plüschke et al. 2001, hereafter COMPTEL MaxEnt) and a homogenous disk model (*right*, hereafter Homo Disk, constant brightness along longitudes, exponential-like in latitudes with scale height 200 pc) for the inner Galaxy as the input sky models in the model fitting.

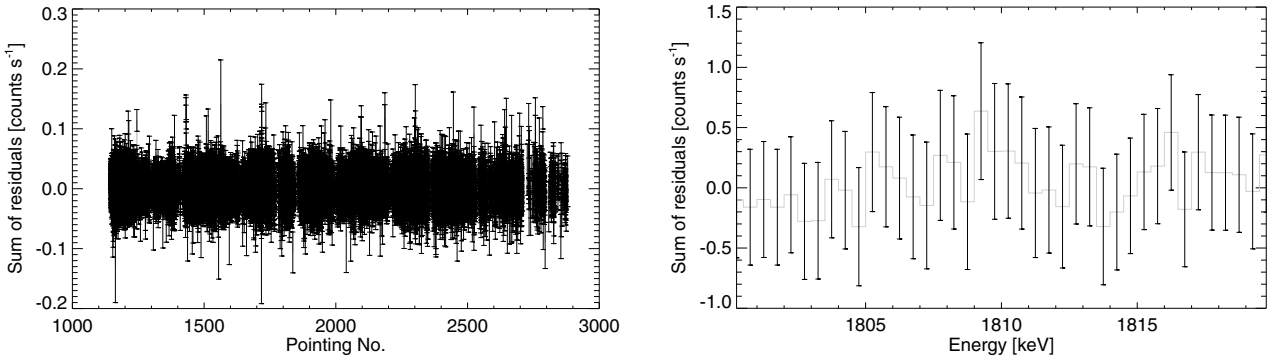

Fig. 4. Residuals versus time (pointings, per 30 min, *left*) and energies (*right*) after model fitting of the inner Galaxy region for the SE database. Residuals around zero confirm that our background models are adequate, with χ^2/d.o.f. = 0.958 in model fittings.

in particular to determine probability constraints for the celestial ^{26}Al line broadening from kinematics. This parameter challenges the spectral resolution of our instrument (about 3 keV at the ^{26}Al line energy), hence so far is bounded from above only. Such asymmetric parameter probability distributions may be far from Gaussian, hence require such more sophisticated treatment (Kretschmer et al. 2009, in preparation).

3. ^{26}Al in the inner Galaxy – an update

The spectral characteristics of ^{26}Al emission in the inner Galaxy serve to study the current nucleosynthesis activity and the properties of the interstellar medium near the ^{26}Al sources on a large-scale averaged scale. We define the "inner Galaxy" as the region $-30° < l < 30°$, $-10° < b < 10°$), and may use this as a representative region for this purpose, since it coincides with the bright ridge of observed 1809 keV emission as observed along the plane of the Galaxy. We specifically exclude regions at higher longitudes such as Cygnus: this region in particular has been recognized as special, in its supernova to Wolf-Rayet ratio, for example (Knödlseder et al. 2004); other emission at large longitudes also may be deviant from the Galactic average and over-emphasized because nearby. We therefore believe that using the $-30° < l < 30°$ region will give us a more representative picture of ^{26}Al source environments in the Galaxy.

Fitting our set of observations to the sky intensity distribution of the ^{26}Al maximum entropy image (MaxEnt) from COMPTEL (Fig. 3, left), we obtain the updated inner-Galaxy ^{26}Al emission spectrum shown in Fig. 5. MaxEnt is one possible sky intensity distribution compatible with the COMPTEL data. The ^{26}Al line is detected at $\sim 28\sigma$ significance.

The ^{26}Al gamma-ray flux from the inner Galaxy turns out as $(2.93 \pm 0.15) \times 10^{-4}$ ph cm^{-2} s^{-1} rad^{-1}. This is consistent with our earlier values $(3.3 \pm 0.4) \times 10^{-4}$ ph cm^{-2} s^{-1} rad^{-1} (Diehl et al. 2006a,b), and also with the COMPTEL imaging-analysis value of $(2.8 \pm 0.4) \times 10^{-4}$ ph cm^{-2} s^{-1} rad^{-1} (Plüschke et al. 2001). The above value is derived using an asymmetric line shape as best matching our expectations from SPI's spectral response and eventual additional celestial line broadening the total ^{26}Al gamma-ray flux of the Gaussian fit as determined for the inner Galaxy region is $(2.73 \pm 0.17) \times 10^{-4}$ ph cm^{-2} s^{-1} rad^{-1}.

In our model-fitting approach to derive ^{26}Al spectra from SPI spectra per pointing (Eq. (1)), the adopted sky distribution models may affect the ^{26}Al flux and line shape results. We estimate the variations and potential systematic uncertainties introduced by the spatial distribution model of the ^{26}Al emission through variation of this sky distribution model within a plausible range.

Our "standard" is the measurement of ^{26}Al gamma-ray emission directly, from COMPTEL. Uncertainties from COMPTEL imaging analysis have however been shown to allow for a range of images which are consistent with the COMPTEL measurements (Knödlseder et al. 1999). We consider the MaxEnt image the compromise between making use of COMPTEL's imaging resolution of about 3.8° (*FWHM*) and the attempts to suppress artifacts from statistical noise. A more conservative COMPTEL image is obtained from the Multi-resolution Expectation Maximization method (MREM), which carefully eliminates noise contributions at each iteration and builds up the image starting from large spatial scales, terminating once the image obtained does not need further refinement in this statistical sense (Knödlseder et al. 1999; Knödlseder 1999). The smooth MREM image from COMPTEL also shows the inner Galactic ridge as well as Cygnus being bright in ^{26}Al emission, yet does not show the few-degree scale features of the MaxEnt map; we consider these two maps as adequate tests for systematics from the range of direct ^{26}Al measurements.

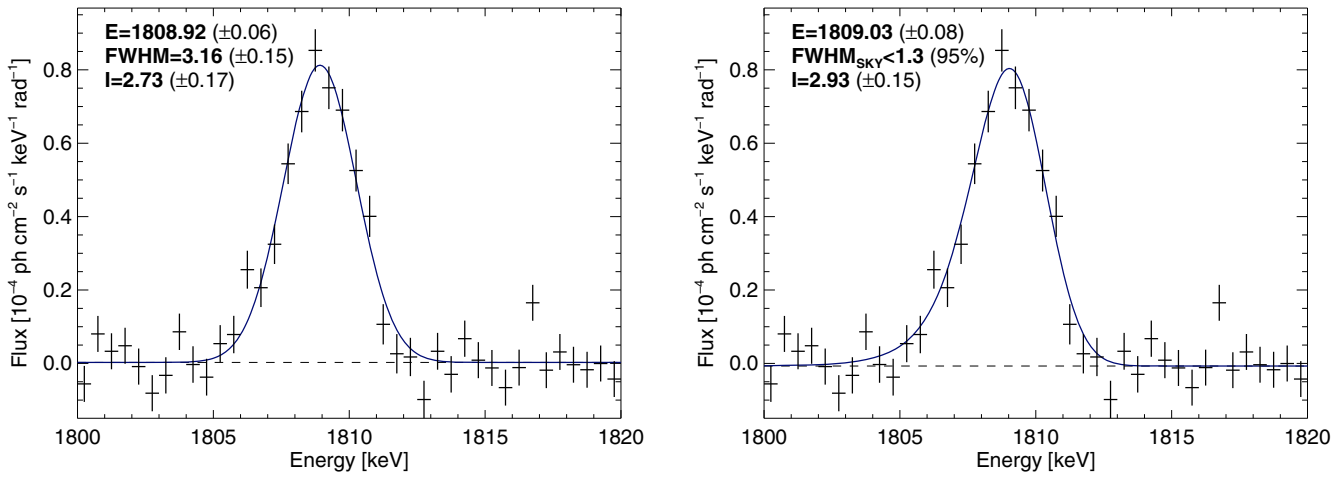

Fig. 5. Spectrum derived from sky model fitting using the COMPTEL ^{26}Al Maximum Entropy image. The left figure shows the ^{26}Al line fitted with a Gaussian, the width of ~3.16 keV (*FWHM*) being consistent with instrumental line widths around 1.8 MeV. The right figure shows the line fitted with a composite line-shape model using the time-averaged instrumental response as it results from cosmic-ray degradation and annealings during the time of our measurement, convolved with a Gaussian representing the cosmic (intrinsic) ^{26}Al line width. The latter is found to be (<1.3 keV, 2σ). Both fits find that the line is intrinsically narrow. Systematic variations of derived line fluxes using two spatial models are less than the statistical uncertainty in the measurement (fluxes are quoted in units of 10^{-4} ph cm^{-2} s^{-1} rad^{-1}).

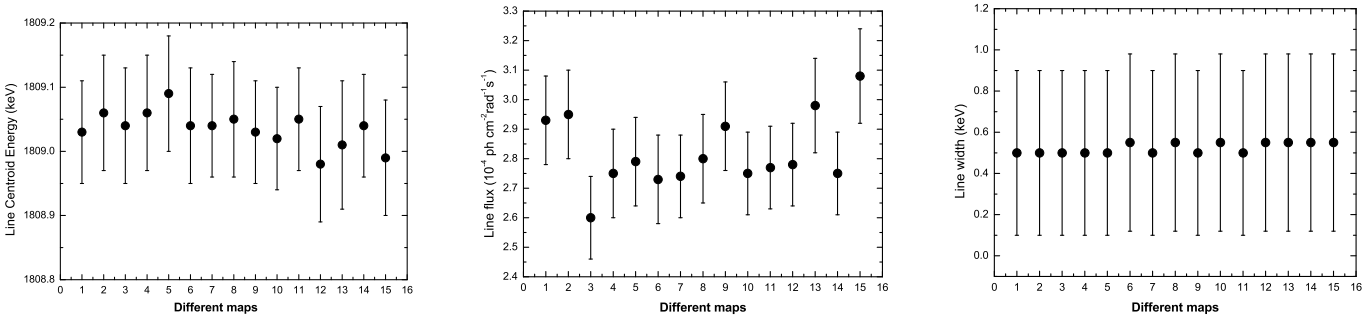

Fig. 6. Comparison of the three line parameters (centroid energy, flux, width, with 1σ error bars) derived in model fittings for different distribution models: 1. COMPTEL maximum entropy ^{26}Al emission map (Plüschke et al. 2001); 2. COMPTEL MREM ^{26}Al emission map (Plüschke et al. 2001); 3. an exponential disk model (scale radius 4 kpc, scale height 180 pc); 4. a homogenous disk model (Fig. 3); 5. HI (Dickey & Lockman 1990); 6. CO (Dame et al. 1987); 7. radio 408 MHz (Haslam et al. 1995); 8. DIRBE/COBE 240 μm (Bennett et al. 1996); 9. IRAS 12 μm (Wheelock et al. 1991); 10. EGRET (>100 MeV, Hunter et al. 1997); 11. a young disk model (Robin et al. 2003); 12. the free electron density distribution model (TC93, scale height 150 pc, Taylor & Cordes 1993) 13. TC93, scale height 300 pc; 14. the free electron density distribution model (NE2001, scale height 140 pc, Cordes & Lazio 2002); 15. NE2001, scale height 330 pc.

Considering the limitations of gamma-ray telescopes, it has been plausible to alternatively use maps obtained in astronomically-more developed wavelength bands, once it it clear that those trace ^{26}Al sources in the Galaxy. Detailed studies have shown (Knödlseder et al. 1999; Diehl et al. 1996) that among the best tracers of ^{26}Al sources are (1) the infrared emission of warm dust grains, mapped with the COBE/DIRBE and arising from radiative heating of dust around clusters of massive stars (Bennett et al. 1996); and (2) radiation of free electrons (free-free emission, Bremsstrahlung) observed at radio frequencies with the WMAP satellite, arising from the ionizing massive-star radiation around massive star clusters. From astrophysical arguments, also maps of interstellar gas in different forms should trace the locations and space density of ^{26}Al sources. (3) Molecular gas is observed through CO line emission at radio frequencies, and has been mapped in rather fine resolution (Dame et al. 1987, 2001); (4) atomic hydrogen (HI) sky surveys have been accumulated (e.g. Dickey & Lockman 1990); and (5) cosmic-ray interactions with interstellar gas produces penetrating continuum gamma-ray emission which has been mapped in the EGRET sky survey (Hunter et al. 1997).

Finally, analytical models for the distribution of ^{26}Al sources have been constructed, based on above knowledge of Galactic structure in its different components (Robin et al. 2003), properly weighted from astrophysical arguments. (6) Double-exponential functions (in galactocentric radius, and scale height above the Galactic plane) have been constructed, as well as more sophisticated models including (7) spiral structure components and building on the distribution of free electrons in the Galaxy as derived from pulsar dispersion measurements (Taylor & Cordes 1993; Cordes & Lazio 2002). The scale height of ^{26}Al sources has been found to lie between the molecular disk (about 50 pc) and the thick disk (about 0.3−1 kpc), with plausible values around 200 pc.

We compare ^{26}Al line spectra determined from these different models and tracers of ^{26}Al sources in the Galaxy. Fifteen different sky distribution maps have been analyzed, and variations on ^{26}Al brightness, ^{26}Al line centroid and width parameters are shown in Fig. 6. Systematic variations are within statistical uncertainties, when we vary the spatial models for ^{26}Al emission. We use their scatter to estimate a "systematic" uncertainty, which turns out as $(2.9 \pm 0.2) \times 10^{-4}$ ph cm^{-2} s^{-1} rad^{-1},

1809.0 ± 0.09 keV, 0.5 ± 0.45 keV for the flux, centroid, and width parameters (with 1σ error bars), separately.

As before (Diehl et al. 2006a), we convert our measured ^{26}Al intensity into an estimate of the total current ^{26}Al mass in the Galaxy, using an assumed geometrical source-distribution model to extrapolate across the entire Galaxy from our inner-Galaxy normalization of such a model, as discussed above. This is required because the flux to mass conversion relies on ^{26}Al source distances, not measured directly in projected sky brightness distribution maps. Several three-dimensional distribution models are applied and compared here, e.g., an exponential disk model, a "young-disk" model, a geometrical representation based on dust emission, and a multi-component model including spiral-arm structures and based on abundances of free electrons in interstellar space. We vary scale height parameters of the appropriate components to also study the latitude extent of the ^{26}Al emission. In all models, we have taken the distance of the Sun to the Galactic center as R_0 = 8.5 kpc (^{26}Al mass sensitively depends on R_0, smaller R_0 will globally reduce the size of the Galaxy, and result in the smaller amount of ^{26}Al).

The average measured ^{26}Al flux of (2.9 ± 0.2) × 10^{-4} ph cm^{-2} s^{-1} rad^{-1} for the inner Galaxy thus translates into a Galactic ^{26}Al mass of (2.7 ± 0.7) $M_\odot$ using a plausible scale height of 180 pc. If we ignored the ejection of ^{26}Al into surrounding cavities and corresponding champagne flows (see our own scale height determination below), and used the lower scale heights of O stars or of the molecular disk, we would obtain lower total amounts around or even below 2 $M_\odot$. This emphasizes the need for spatially-resolved ^{26}Al studies (see Sect. 5 and Fig. 12 below). The quoted uncertainty here includes both the statistical uncertainty as propagated from the fitting method, and the systematical uncertainty derived from variations among plausible representations of the sky distribution of the emission plus alternative 3-dimensional ^{26}Al source distribution models (see also Fig. A4.1 in Supplemental materials of Diehl et al. 2006a).

The line width of ^{26}Al conveys global information about the spread in projected velocities of ^{26}Al nuclei when they decay and emit characteristic 1809 keV gamma-rays. Astrophysical origins of ^{26}Al line width may come from two effects: random motions in the interstellar medium (Chen et al. 1997) and Galactic differential rotation (Kretschmer et al. 2003). A line broadening of ∼1 keV from our line-shape constraints corresponds to thermal Doppler velocities of ∼120 km s^{-1}.

The Gaussian used to represent the ^{26}Al line (Fig. 5 left) shows a width of 3.16 ± 0.15 keV (*FWHM*), consistent with the instrumental width determined as ∼3.1 keV near 1809 keV from nearby instrumental lines at 1764 and 1779 keV. This indicates that the cumulative ^{26}Al line emission in the inner Galaxy is intrinsically rather narrow in energy around the laboratory value, with little kinematic Doppler broadening, well below SPI's energy resolution.

For such a strong signal, we can be more ambitious, however, and attempt to quantitatively constrain the intrinsic (celestial) line broadening in a statistical probability analysis as described above (see also Diehl et al. 2006b; Kretschmer et al. 2004). We know the instrumental line response of our instrument at each epoch of the mission from detailed studies of a large number of instrumental lines. The response gradually degrades and develops an increasing tail component on the low-energy side of the photopeak energy, due to incomplete charge collection as the detector's Ge lattice experiences damaging from cosmic-ray impacts. Annealings restore better charge collection and a symmetric instrumental-line response whose width is determined and dominated by statistics of the charge collection. We assemble the effective instrumental-line response for our study through appropriate weightings of these time-dependent responses. Then we fit the convolution of a parameterized Gaussian with this response shape function, and thus derive values for the celestial ^{26}Al line centroid energy and broadening. MCMC sampling of the probability distributions of these parameters then allows us to translate the parameter value uncertainties into probability constraints by integrating over these distributions. In particular, the probability distribution of the intrinsic width may not peak at zero, indicating a small but by itself non-detectable broadening of the line. In this case, our approach yields a reliable estimate of the upper bound on line broadening, which is the astrophysically-relevant quantity to constrain kinematics of decaying ^{26}Al nuclei in the interstellar medium. The fitted parameters are the line centroid, the intrinsic width of celestial ^{26}Al , the intensity of the line, and two parameters for the underlying continuum (see Fig. 5 right). The intrinsic line width is now constrained to <1.3 keV (2σ, which is consistent and yet significantly smaller than the earlier constraints based on fewer SPI data (Diehl et al. 2003, 2006b).

In the inner Galaxy, Galactic differential rotation alone can lead to significant Doppler shifts towards specific longitudes where the projected-velocity differences with respect to the solar orbit reach maxima; line broadening results if we integrate over a larger longitude range with different bulk velocity differences. Kretschmer et al. (2003) have simulated the ^{26}Al line shape diagnostics in the inner Galaxy due to Galactic rotation and ^{26}Al ejection from sources, and find that line broadening of up to 1 keV is expected if the signal is integrated over the inner region of the Galaxy. Our present large-scale line-shape constraints are consistent with these expectations.

If we interpret line broadening of the ^{26}Al line from the inner Galaxy in terms of interstellar-medium characteristics, the intrinsic-width constraint of <1.3 keV corresponds to 160 km s^{-1} as a corresponding 2σ limit on ISM velocities. This is well within the plausible and acceptable range for the environment of normal interstellar-medium turbulence (Chen et al. 1997), leading us to conclude that, within uncertainties, the average velocities of decaying ^{26}Al in the Galaxy are not abnormally-high (compare discussion after Naya et al. 1996; in Chen et al. 1997).

In summary, the measured line width of ^{26}Al from the inner Galaxy is consistent with Galactic rotation and modest interstellar-medium turbulence around the sources of ^{26}Al . This confirms earlier results on the ^{26}Al line width from HEAO-C (Mahoney et al. 1984), RHESSI (Smith 2003), and SPI on INTEGRAL (Diehl et al. 2006b). The GRIS balloon experiment had reported a very broad line with a width ∼5.4 keV (Naya 1996), which is inconsistent with these measurements and clearly ruled out. This is reassuring: within uncertainties, the average velocities of decaying ^{26}Al in the Galaxy are not abnormally-high (see discussion in Chen et al. 1997).

The relative position of the ^{26}Al gamma-ray line centroid with respect to the laboratory-determined ^{26}Al decay energy value of 1808.65 ± 0.07 keV (Firestone & Ekström 2004) yields information on potential bulk motion of ^{26}Al in the Galaxy. The ^{26}Al line centroid energy from the whole inner Galaxy is determined at 1808.92 ± 0.06 keV from the Gaussian fit and 1809.03 ± 0.08 keV from the instrumental-response-convolved fit, even after considering uncertainties, the measured centroid energy is higher than the laboratory value. The effect of this blueshift for the whole inner Galaxy will be discussed below.

In our determination of ^{26}Al line properties, we represent the spectra derived from detailed model fitting by a line component for ^{26}Al plus a linear component which could capture any

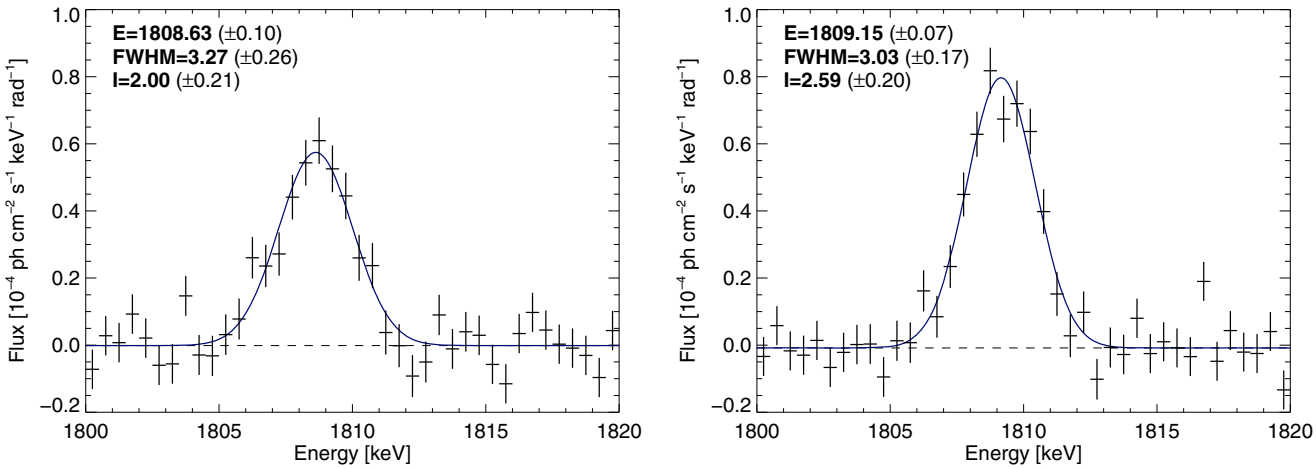

Fig. 7. ^{26}Al spectra for two Galactic quadrants (*left* $0° < l < 60°$, and *right* $-60° < l < 0°$). Line centroids relative to the centroid energy of ^{26}Al line in the laboratory (1808.65 keV) show a significant blueshift in the 4th quadrant. Both the spectra have width values near the value of the instrumental line width, implying that ^{26}Al emissions from two quadrants are the narrow lines. In addition, the ^{26}Al flux of the 4th quadrant is higher than that of the 1st quadrant, and the flux ratio is ∼1.3.

underlying systematics in our background or sky modellings. We expect that our adjacent-energy background model component will eliminate Galactic continuum emission, at least to first order, if the spectral shape is rather flat across our 40 keV energy range (1785−1826 keV). The diffuse gamma-ray continuum in the inner Galaxy is $\sim 2 \times 10^{-6}$ ph cm^{-2} s^{-1} rad^{-1} keV^{-1} in the energy band of 1−2 MeV (Strong et al. 1999). Indeed, we find that offsets above zero in our spectra are rather small and negligible, supporting this property of our background model.

4. ^{26}Al emission along Galactic longitudes

The 9-year COMPTEL imaging of ^{26}Al line emission had already suggested some asymmetry in the inner Galaxy: the fourth Galactic quadrant appears somewhat brighter than the first quadrant (Plüschke (2000), finds a significance of 2.5σ for a brightness difference). COMPTEL could provide the image details of ^{26}Al in the Galaxy, but no significant spectral information due to its spectral resolution of about 150 keV near the ^{26}Al line. SPI with its Ge detectors features sufficiently-high spectral resolution to allow astrophysical constraints from ^{26}Al line shapes, averaged over the Galaxy as discussed above, but also for different regions along the Galactic plane due to its imaging properties as a coded-mask telescope.

In this section, we will proceed towards increasing spatial resolution along the Galactic plane, starting out from testing Galactic asymmetries between the first and fourth quadrant. ^{26}Al line parameters toward the different directions of the Galactic plane are determined using separate sky maps covering each sky region, simultaneously fitting these together with our background model to the entire sky survey database. ^{26}Al line fluxes, centroid energies, and line widths then are derived by a simple Gaussian fit to the ^{26}Al line in the resulting spectra, as we are interested in relative changes between different portions of the sky. This will allow us to identify line shifts from bulk motion such as expected from large-scale Galactic rotation, and hints for additional line broadenings in particular regions, which would reflect increased ^{26}Al velocities in such regions. A homogenous disk model (see Fig. 2 right, $-60° < l < 60°$, $-10° < b < 10°$, scale height 200 pc) is used here to avoid a bias of sky distribution models along the Galactic plane, for such relative comparison.

^{26}Al spectra for the 1st ($0° < l < 60°$) and 4th quadrant ($-60° < l < 0°$) are presented in Fig. 7. In the 4th quadrant we note a blueshift of 0.49 ± 0.07 keV relative to the centroid energy of ^{26}Al line in the laboratory, but no significant redshift in the 1st quadrant is apparent (∼0.04 ± 0.10 keV). Both spectra have width values compatible with no significant ^{26}Al line broadenings. The indicated ^{26}Al asymmetry between the two inner Galactic quadrants appears again, with a flux ratio of ∼1.3 ± 0.2.

We proceed further towards more confined Galactic regions using four sub-maps with 30 degree width along Galactic longitude, to obtain ^{26}Al spectra for these regions shown in Fig. 8: (1) $0° < l < 30°$; (2) $30° < l < 60°$; (3) $-30° < l < 0°$; and (4) $-60° < l < -30°$. Centroid energy shifts of the ^{26}Al line are found, +0.15 ± 0.12 keV and −0.61 ± 0.09 keV in regions (1) and (3) respectively, as expected from large-scale Galactic rotation. The inner region ($-30° < l < 30°$) is seen to be much brighter than the two outer regions of the Galaxy, consistent with the COMPTEL ^{26}Al map (note that here we use a homogeneous sky distribution model as the model-fitting prior). The indicated ^{26}Al emission asymmetry for the 1st and 4th quadrants also shows up again between regions (3) and (1), with a flux ratio of ∼1.15 ± 0.18. Even further out, region (4) may also be brighter than (2) by ∼1.6 ± 0.6. Since smaller regions include less ^{26}Al signal, these differences are, however, not significant.

Challenging the imaging capability of SPI for diffuse and extended emission, we refine spatial structure even more towards smaller longitude intervals. In Fig. 9, we show a spectrum representing the Galactic center region ($-5° < l < 5°$, $-10° < b < 10°$), where the ^{26}Al line is still significant (>4σ). The line centroid energy is determined at 1808.58 ± 0.27 keV, and is consistent with the laboratory value – no line shift from bulk motion is indicated.

Then we also derive spectra for six smaller longitude intervals of 20 degree width along the Galactic plane ($-60° < l < 60°$, see Fig. 10). The ^{26}Al line is still detected for the inner Galaxy ($-40° < l < 40°$, >6σ for each 20° bin region), but only marginal for the two outer regions ($40° < l < 60°$ and $-60° < l < -40°$, <4σ). This may be attributed to both less ^{26}Al brightness and to less exposure in these regions, compared to the inner Galaxy.

For the four inner regions, ^{26}Al line centroid shifts are observed. When we use the ^{26}Al line centroid energy of

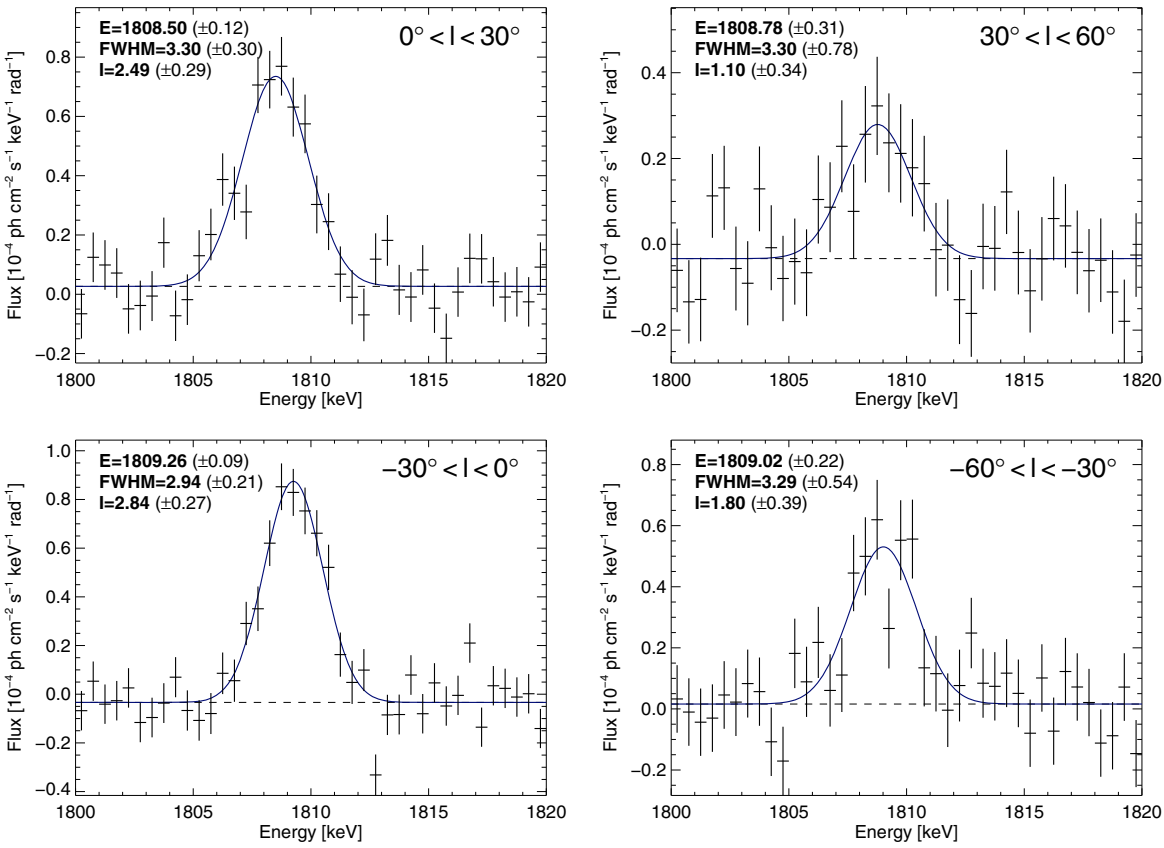

Fig. 8. ^{26}Al spectra of four segments along the Galactic plane ($-60° < l < 60°$).

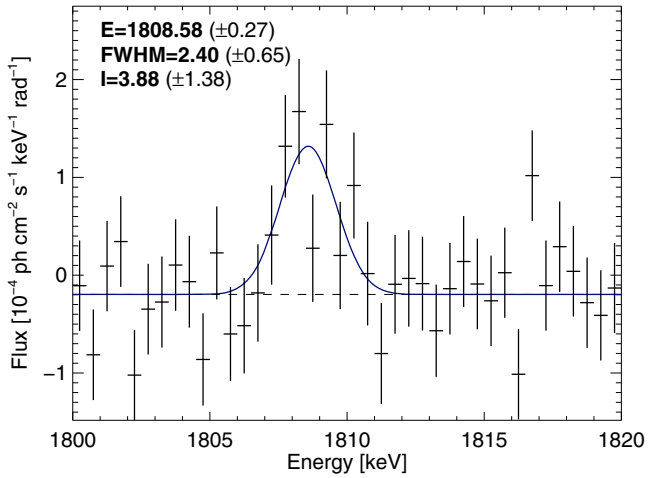

Fig. 9. ^{26}Al spectrum from the Galactic center ($-5° < l < 5°$, $-10° < b < 10°$). The determined line centroid energy (1808.58 ± 0.27 keV) is consistent with the laboratory value.

1808.65 keV from the laboratory as a reference (rather than our own determination, Fig. 9), we obtain ^{26}Al line centroid energy shifts along Galactic longitudes as shown in Fig. 11. Evidently, towards positive longitudes of ∼0°−40°, the redshift in energy is minor, ∼0.1 keV, while for negative longitudes, the blueshift is substantial, ∼0.4 keV for $-20° < l < 0°$ and up to 0.8 keV for $-40° < l < -20°$. This asymmetry of ^{26}Al line energy shifts along the Galactic plane is inconsistent with simple azimuthally-symmetric Galactic rotation; it is clear evidence for pronounced spiral-arm structure in the inner Galaxy, and possibly peculiar bulk motion along the Galaxy's bar (e.g. Englmaier & Gerhard 1999; Hammersley et al. 2007, and references therein).

Figure 11 shows the intensity distribution of ^{26}Al emission (from the same 20° regions, Fig. 10) along the Galactic plane, adding the (longitude-range normalized) Galactic-Center region ^{26}Al intensity ($|l| < 5°$, Fig. 9) for comparison. The variability of ^{26}Al intensity along the Galactic plane again is evident.

We note that the ^{26}Al line in the region of $20° < l < 40°$ appears somewhat broadened, with a Gaussian width of $FWHM \sim 4.15 \pm 0.75$ keV (also see Fig. 11). This may hint towards a peculiar ^{26}Al source region towards this direction, which could be associated with the Aquila region (Rice et al. 2006). Broadening could result from higher turbulence if the ^{26}Al source region is younger than average and dominated by the ^{26}Al ejection from more massive stars (see Knödlseder et al. 2004). Further studies would be interesting, and have the potential to identify star formation otherwise occulted by foreground molecular clouds.

5. Latitudinal variations of ^{26}Al emission

The interpretation of ^{26}Al imaging and spectral results relies on (uncertain) distances of ^{26}Al sources. Along the line-of-sight, the detected ^{26}Al signal could originate from local star-formation complexes (∼100 pc), or from the nearest part of the Sagittarius-Carina arm (1−2 kpc), or from the Galactic center region (∼8 kpc), or even from the distant side of the Galaxy (>10 kpc).

In this section, we explore a possibility to resolve the ^{26}Al signals for local complexes from the large scales of the Galaxy through different latitudinal signatures. For such analysis, we split a homogenous-disk model (Fig. 3 right) into submaps along Galactic latitudes, and derive separate ^{26}Al spectra

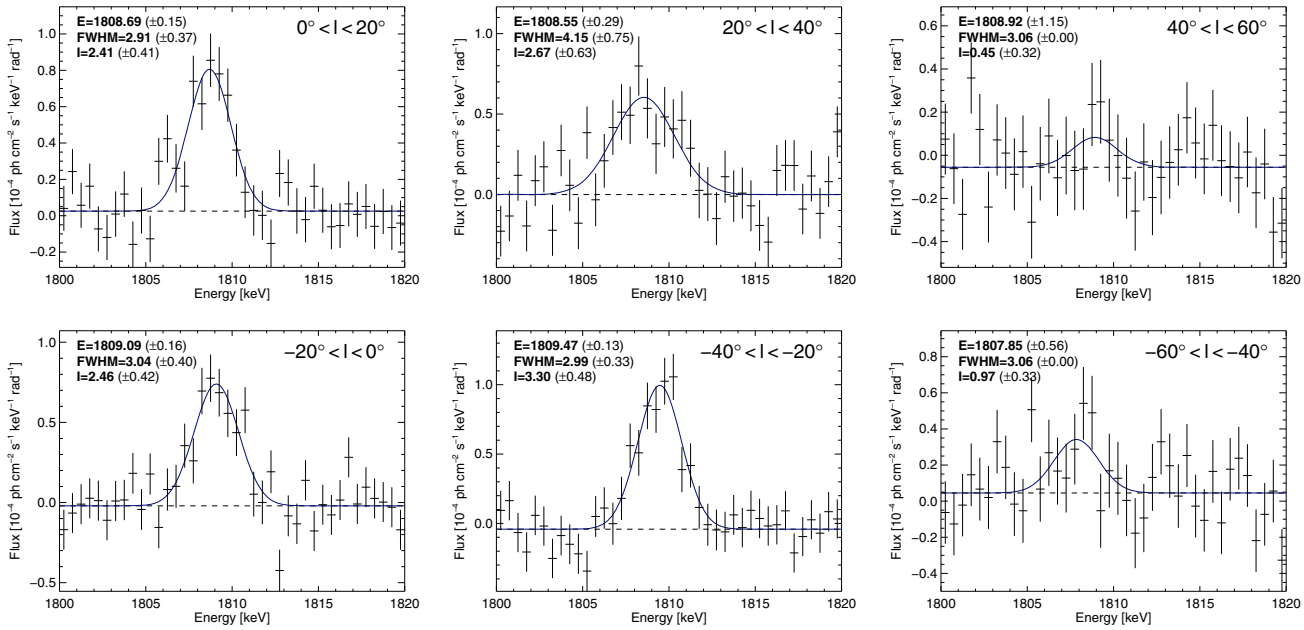

Fig. 10. ^{26}Al spectra of six segments along the Galactic plane ($-60° < l < 60°$). Small longitude degree bin (20°) makes the detections of ^{26}Al not significant in the regions of $40° < |l| < 60°$.

for the different latitude ranges simultaneously through model fitting to our observations. We study the ^{26}Al emission for three intervals along latitudes, $-5° < b < 5°$ (low latitudes), $5° < b < 20°$ and $-20° < b < -5°$ (intermediate latitudes). ^{26}Al emission for low latitudes ($|b| < 5°$) should be dominated by a large-scale origin in the Galactic disk, while ^{26}Al emission at higher latitudes ($|b| > 5°$) could originate from more local star-formation systems such as OB associations in the Gould Belt. This definition is similar to the one used in pulsar population studies (Wang et al. 2005). The Gould Belt is an ellipsoidal shaped ring-like structure delineated by the groups of nearby stellar groups within ≃1 kpc, with semi-major and minor axes of ∼500 pc and 340 pc, respectively (Perrot & Grenier 2003). The center of this structure is located towards $l = 130°$, displaced from the Sun's location by about 200 pc (Guillout et al. 1998). The Vela region is located near the outer boundary of the Gould Belt towards $l \sim -90°$. The nearby Sco-Cen region at about 140 pc distance towards $l \sim -10°$, $b \sim 10°$ probably also belongs to the Gould Belt. The origin of this structure is debated, between triggered sequential star formation propagating outwards from its center, and an external triggering event such as a high-velocity cloud falling through the Galaxy's plane (see Perrot & Grenier 2003; Pöppel 1997).

Figure 12 displays the ^{26}Al intensity distribution along Galactic latitudes for $|l| < 60°$. No ^{26}Al signal is detected at negative latitudes ($-20° < b < -5°$), while weak ^{26}Al emission is detected at positive latitudes ($\sim 2\sigma$, $5° < b < 20°$). We also derive latitudinally-separated ^{26}Al emission for the 1st and 4th quadrants separately again through model fitting, also shown in Fig. 11. No ^{26}Al signal is detected for off-plane regions of the 1st quadrant, while in the 4th quadrant, ^{26}Al emission is still clearly detected (3σ) in the latitude region $5° < b < 20°$. This ^{26}Al emission towards $b > 5°$, $l < 0°$ could be attributed to the nearby Sco-Cen star-formation complex at ≃140 pc distance.

We also determine the scale height of the Galactic plane in ^{26}Al emission by comparing the fit quality for sets of two different plausible geometrical models for the ^{26}Al source density distribution in the Galaxy, varying their scale height parameter (Fig. 12 right). We use a Galactocentric double-exponential disk model (ExpDisk) described by

$$\rho(R, z) \propto \mathrm{e}^{-\left(\frac{R}{R_0}+\frac{|z|}{z_0}\right)}, \quad (2)$$

where R is the Galactocentric distance within the plane, and z is the height above the plane, with $R_0 = 3.5$ kpc and z_0 as the scale radius and height parameter. Alternatively, we use a model which includes the spiral-arm structure of the Galaxy as derived by Taylor & Cordes (1993); we use only their components for the inner Galaxy and the spiral arms, with identical scale height parameter (in this model, the density perpendicular to the disk is described as $\mathrm{sech}(z/z_0)$). In order to avoid a bias from bright special regions such as Cygnus/Vela/Carina, we restrict this analysis to data within $|l| < 60°$ and $|b| < 30°$. Figure 12 (right) shows the variation of log-likelihood values with different scale heights for both model types. Here, the values for the exponential-disk models have been shifted by +16, as the spiral-arm model systematically provides a better description of our data. With $-2 \log L$ being asymptotically χ^2 distributed, we derive a scale height of 130^{+120}_{-70} pc (1σ) for the ^{26}Al emission in the inner Galactic disk, from the spiral arm model constraints. This confirms previous such studies based on COMPTEL data (Diehl et al. 1998).

6. Summary and conclusions

The study of the ^{26}Al line and its details in different regions of the Galaxy is one of the main goals of the SPI spectrometer on INTEGRAL. Using five years of SPI data, we find the ^{26}Al signal from the inner Galaxy ($|l| < 30°$, $|b| < 10°$) with a high significance of $\sim 28\sigma$. The ^{26}Al flux integrated over the inner Galaxy of $(2.9 \pm 0.2) \times 10^{-4}$ ph cm^{-2} s^{-1} rad^{-1} is consistent with our own and other earlier measurements, though significantly lower than the ones from measurements with instruments which have even more modest spatial resolution on the sky (see Fig. 2 of Diehl et al. 2004). Taking the distance of the Sun to the Galactic center as $R_0 = 8.5$ kpc, we convert the measured ^{26}Al flux to a Galactic ^{26}Al mass of $(2.7 \pm 0.7)\ M_\odot$. We compared different plausible

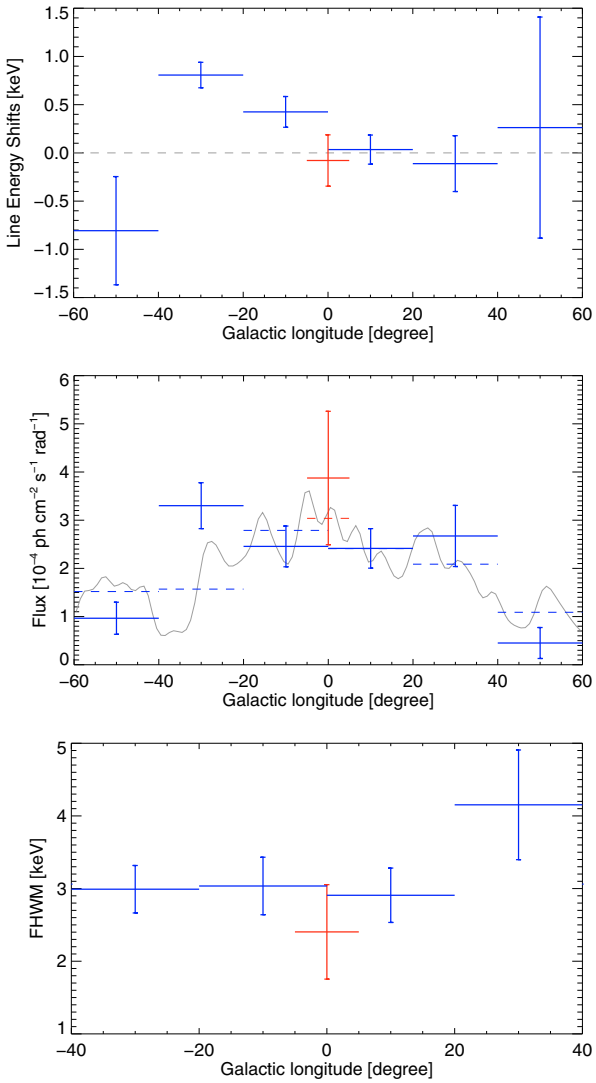

Fig. 11. *Top*: ^{26}Al line energy shifts along the Galactic plane ($-60° < l < 60°$, with longitude bin widths of 20°, ^{26}Al spectra from Fig. 10) relative to the line centroid of the ^{26}Al line (fitted energy 1808.65 keV). *Center*: ^{26}Al intensity distribution along the Galactic plane (from Figs. 9, 10). For comparison, the COMPTEL-derived ^{26}Al intensity profile is shown (solid line, and dashed lines when integrated over the same longitude bins). *Bottom*: ^{26}Al *FWHM* (Gaussian fitting) variation along the Galactic longitudes, a broad ^{26}Al line feature is detected toward the longitudes $20° < l < 40°$.

models for the sky distribution of ^{26}Al emission and how it may affect the global ^{26}Al flux measurement. We find that different sky distribution models do not substantially affect ^{26}Al intensity and line shapes for the integrated inner Galaxy, and we have used the observed variations of ^{26}Al mass values to estimate a systematic uncertainty, added to the statistical uncertainty from the model fitting, to yield the $\pm 0.7\ M_\odot$ uncertainty quoted.

The ^{26}Al line centroid energy appears blue-shifted relative to the laboratory value of 1808.65 ± 0.07 keV if integrated over the inner Galaxy (1809.0 ± 0.1 keV). With refined spatial resolution this turns out to be mostly due to asymmetric bulk motion which we find along the plane of the Galaxy, and attribute to asymmetries in inner spiral arms and to the Galaxy's bar. In particular, for the central longitude bin towards the Galactic Center, the signal is strong enough to allow for a rather small longitude range integration, and we find a ^{26}Al line centroid consistent with the laboratory value and thus with the absence of bulk motion relative to the Sun. Also, here the ^{26}Al line appears as most-narrow with an upper limit of 1.3 keV (2σ). The measured line width of ^{26}Al from the large-scale integrated inner Galaxy with an upper limit of 1.3 keV (2σ) is consistent with expectations from both Galactic rotation and modest interstellar-medium turbulence around the sources of ^{26}Al (turbulent velocities constrained below 160 km s^{-1} even when disregarding the effects of galactic rotation). Our line width results are consistent with previous reports by HEAO-C (Mahoney et al. 1984), RHESSI (Smith 2003), but the very broad line with a width ~5.4 keV reported by GRIS (Naya et al. 1996) is clearly ruled out by our SPI measurements (4σ significance level).

From our study of ^{26}Al emission in spatially-restricted regions along the plane of the Galaxy, we find:

- ^{26}Al brightness appears asymmetric for the two inner quadrants, with a flux ratio of the 4th quadrant to the 1st of ~1.3 ± 0.2 (Fig. 7).
- The ^{26}Al line energy varies clearly along the Galactic plane (Fig. 11): a minor redshift (~0.1 keV) for positive longitudes, but significant blueshift (~0.4–0.8 keV) for negative longitudes.
- The ^{26}Al line towards the direction of $20° < l < 40°$ shows a hint for additional line broadening.
- The scale height of Galactic-plane ^{26}Al emission is 130^{+120}_{-70} pc (1σ), determined towards the inner Galaxy ($|l| < 60°$).
- There is a strong hint for ^{26}Al emission in the fourth Galactic quadrant at intermediate latitudes $l < 0°$, $b > 5°$ (Fig. 11).

This leads us to several astrophysical implications and the "bar" structures:

- The disk of our Galaxy apparently is not azimuthally-symmetric. The ^{26}Al brightnesses for the two inner quadrants appear different, both from our INTEGRAL and from earlier COMPTEL results, favoring the fourth quadrant. ^{26}Al line shifts towards the blue in such brighter regions are more pronounced than the redshifts on the fainter side of the disk, unexpected from a simple and symmetric Galaxy model and its large-scale rotation properties. These phenomena may reflect variations in the space distribution of young stars, possibly related to the inner parts of the spiral arms and their interfaces to the "molecular ring" and the "bar" structures. Large non-circular motions have been seen in HI and CO observations (Mulder & Liem 1986; Gerhard & Vietri 1986), and also from the NIR light distribution (Binney et al. 1997), in addition to source count asymmetries (Nikolaev & Weinberg 1997) and non-symmetric gas dynamics (Englmaier & Gerhard 1999). The bar is most clearly traced in infrared emission from dust (Marshall et al. 2008), which suggests a position angle of ~25° of the bar with the near end pointing towards us in the first quadrant, and a total length of about 4 kpc. The transition regions between spiral arms and bar are likely to incur star formation (Verley et al. 2007), and affect the dynamics of gas and stars. Simply superimposing a homogeneous star-forming bar to the rotating spiral would, however, not agree with our results – the inner Galaxy structure may be more complex. Localized star-forming regions could lead to peculiar motion of hot gas ejected from winds and supernovae, which might dominate over large-scale Galactic rotation. Such activity could be the cause of the observed asymmetry of the ^{26}Al line intensities and line energy shifts in the inner Galaxy. On the

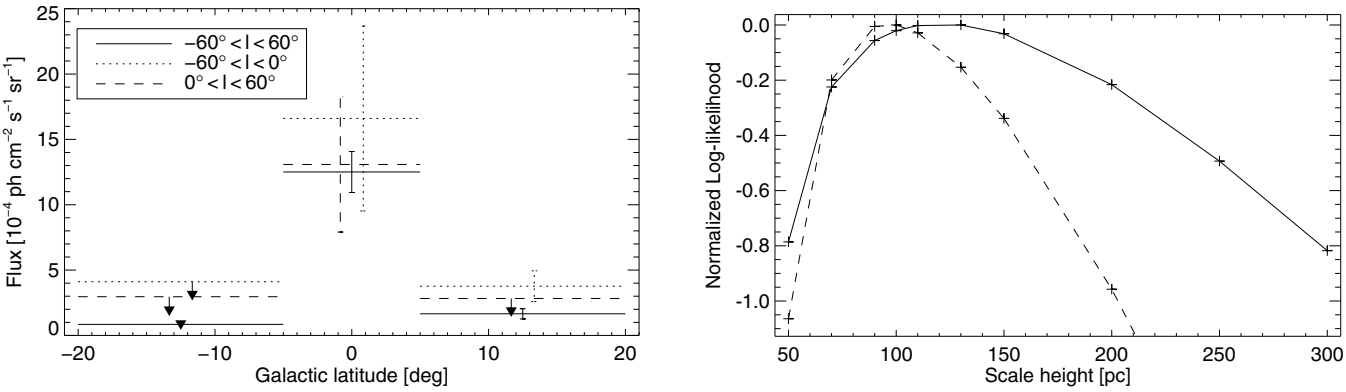

Fig. 12. *Left*: ^{26}Al intensities versus Galactic latitudes (solid lines, $|l| < 60°$). ^{26}Al emission from low latitudes (the Galactic disk) dominates ($|b| < 5°$). For comparison, ^{26}Al intensities for each Galactic quadrant are also shown. Significant ^{26}Al emission is detected towards $b > 5°$, $l < 0°$. *Right*: determination of the Galactic-disk scale height. Shown is the logarithmic likelihood-ratio for the exponential-disk (dashed line) and spiral-arm structure models (solid line) for different scale height values. Log-likelihood values for the exponential-disk model have been offset by +16.

other hand, other more nearby ^{26}Al source regions could be responsible for these irregularities, such as the nearest part of the Sagittarius-Carina arm in the fourth quadrant, or regions/complexes attributed to the Gould Belt such as the Scorpius-Centaurus-Lupus groups. Refined ^{26}Al studies and their combination with astrometry from other tracers of Galactic structure could help to understand the role of our Galaxy's bar.

– The ^{26}Al emission asymmetry (1.3 ± 0.2) between fourth and first quadrant of the Galaxy is lower than the intensity contrast of $1.8^{+0.5}_{-0.3}$ reported for positron annihilation emission from the disk of the Galaxy (Weidenspointner et al. 2008). ^{26}Al by itself releases a positron in 82% of its decays; it is uncertain, however, how this translates into annihilation photons, from the variety of slowing down and annihilation processes which determine the fate of positrons in interstellar space. Both spatial and temporal variations and non-linearities scaling with gas density may occur.
– The scale height of Galactic-plane ^{26}Al emission is significantly larger than the molecular-gas disk scale height of ≃50 pc, yet significantly smaller than the "thick disk" part of the Galaxy. It is consistent with ^{26}Al being ejected from star-forming regions, and partly extending more towards the Galactic halo where gas pressure is lower than within the plane of the Galaxy ("champagne flows").
– Localized regions may deviate in interesting detail from the large-scale averaged properties of ^{26}Al source regions. The direction of $20° < l < 40°$ corresponds to the Aquila region, and our hint for additional line broadening may be due to increased interstellar turbulence from stellar-wind and supernova activity at the characteristic age of stellar groups of that region, which may have created a supershell of substantial size (320 × 550 pc, see Maciejewski et al. 1996). Similar arguments are being explored for the Cygnus region, based on earlier hints of peculiar ^{26}Al emission (Martin et al., in preparation). The hint for ^{26}Al emission at $l < 0°$, $b > 5°$ (Fig. 12) may be attributed to the relatively nearby star forming complexes of the Sco-Cen association (de Geus 1992). Sco-Cen and several nearby stellar groups are attributed to the larger structure of the "Gould Belt", which is suggested to have been more actively forming stars during the last 30 Myr (Grenier 2000; Perrot & Grenier 2003). These examples indicate that spatially-resolved ^{26}Al emission properties may enable new diagnostics of the interactions of massive stars with their surroundings, when combined with other astronomical constraints on cold gas and stars of such regions.

INTEGRAL/SPI will continue to accumulate more data for several years, to cover more sky regions in the outer Galaxy and at intermediate latitudes. This will allow us to deepen the studies reported in this paper, and to refine spatial information on the ^{26}Al line and/or increase the significance of the results reported above, as signal statistics increases and instrumental-background models are tightened. These studies will help us to better understand the properties of ISM near groups of massive stars, and the bulk motion of gas in the inner Galaxy from Galactic rotation and other peculiar kinematics. Nearby ^{26}Al sources may be also discriminated with better exposure towards candidate regions, improving our determination of the ^{26}Al mass in the Galaxy and towards regions where the stellar census is known to a better degree. Studies of ^{26}Al from nearby star-formation regions (e.g., Cygnus, Vela, Sco-Cen, Orion) are a promising diagnostic for the massive star origin of Galactic ^{26}Al and kinematics of ^{26}Al ejecta in ISM. From this, important constraints on massive-star and supernova nucleosynthesis are obtained, refining our models of their complex interiors (see e.g. Woosley & Heger 2007; or Chieffi & Limongi 2006).

Acknowledgements. We are grateful to the anonymous referee for the comments to improve the draft. The INTEGRAL project is supported by government grants in the member states of the hardware teams. The SPI project has been completed under responsibility and leadership of CNES. We are grateful to ASI, CEA, CNES, DLR, ESA, INTA, NASA, and OSTC for support. W. Wang is also supported by the National Natural Science Foundation of China under grant 10803009.

References

Attié, D., Cordier, B., Gros, M., et al. 2003, A&A, 411, L71
Bennett, C. L. 1996, ApJ, 464, L1
Binney, J., Gerhard, O., & Spergel, D. 1997, MNRAS, 288, 365
Chen, W., Gehrels, N., & Diehl, R. 1995, ApJ, 440, L57
Chen, W., Diehl, R., Gehrels, N., et al. 1997, ESA-SP, 382, 105
Cordes, J. M., & Lazio, T. J. W. 2002 [arXiv:astro-ph/0207156]
Courvoisier, T. J.-L., Walter, R., Beckmann, V., et al. 2003, A&A, 411, L53
Dame, T. M., Ungerechts, H., Cohen, R. S., et al. 1987, ApJ, 322, 706
Dame, T. M., Hartmann, Dap, & Thaddeus, P. 2001, ApJ, 547, 792
de Geus, E. J. 1992, A&A, 262, 258
Dickey, J. M., & Lockman, F. J. 1990, ARA&A, 28, 215
Diehl, R., Dupraz, C., Bennett, K., et al. 1995, A&A, 298, 445

Diehl, R., Bennett, K., Dupraz, C., et al. 1996, A&AS, 120, 321
Diehl, R., Oberlack, U., Knödlseder, J., et al. 1998, IAU Colloq., 166, ed. D. Breitschwerdt, M. J. Freyberg, & J. Truemper (Berlin: Springer Verlag), Lecture Notes in Physics, 506, 393
Diehl, R., Knödlseder, J., Lichti, G. G., et al. 2003, A&A, 411, L451
Diehl, R., et al. 2004 [arXiv:astro-ph/0405192]
Diehl, R., Halloin, H., Kretschmer, K., et al. 2006a, Nature, 439, 45
Diehl, R., Halloin, H., Kretschmer, K., et al. 2006b, A&A, 449, 1025
Englmaier, P., & Gerhard, O. E. 1999, MNRAS, 304, 512
Firestone, R. B., & Ekström, L. B. 2004, http://ie.lbl.gov/toi/
Gerhard, O. E., & Vietri, M. 1986, MNRAS, 223, 377
Grenier, I. A. 2000, A&A, 364, L93
Guillout, P., Sterzik, M. F., Schmitt, J. H. M. M., Motch, C., & Neuhaeuser, R. 1998, A&A, 337, 113
Hammersley, P., Garzón, F., Cabrera-Lavers, A., et al. 2007, Rev. Mex. Astron. Astrofis., Ser. conf., 29, 63
Haslam, C. G. T., Salter, C. J., Stoffel, H., & Wilson, W. E. 1995, Astronomy Data Image Library, 1
Hunter, S. D., Bertsch, D. L., Catelli, J. R., et al. 1997, ApJ, 481, 205
Jensen, P. L., Clausen, K., Cassi, C., et al. 2003, A&A, 411, L7
Knödlseder, J. 1999, ApJ, 510, 915
Knödlseder, J., Bennett, K., Bloemen, H., et al. 1999, A&A, 344, 68
Knödlseder, J., Valsesia, M., Allain, M., et al. 2004, ESA-SP, 552, 33
Kretschmer, K., Diehl, R., & Hartmann, D. H. 2003, A&A, 412, L47
Kretschmer, K., Diehl, R., & Hartmann, D. H. 2004, ESA-SP, 552, 103
Leleux, P., Albernhe, F., Borrel, V., et al. 2003, A&A, 411, L85
Limongi, M., & Chieffi, A. 2006, ApJ, 647, 483
Maciejewski, W., Murphy, E. M., Lockman, F. J., & Savage, B. D. 1996, ApJ, 469, 238
Mahoney, W. A., Ling, J. C., Jacobson, A. S., & Lingenfelter, R. E. 1982, ApJ, 262, 742
Mahoney, W. A., Ling, J. C., Wheaton, W. A., & Jacobson, A. S. 1984, ApJ, 286, 578
Marshall, D. J., Fux, R., Robin, A. C., & Reylé, C. 2008, A&A, 477, L21
Mulder, W. A., & Liem, B. T. 1986, A&A, 157, 148
Naya, J. E., Barthelmy, S. D., Bartlett, L. M., et al. 1996, Nature, 384, 44
Nikolaev, S., & Weinberg, M. D. 1997, ApJ, 487, 885
Perrot, C. A., & Grenier, I. A. 2003, A&A, 404, 519
Plüschke, S. 2000, Ph.D. Thesis, Technische Universität München
Plüschke, S., Diehl, R., Schönfelder, V., et al. 2001, ESA-SP, 459, 55
Pöpple, W. 1997, Fundamentals of Cosmic Physics, 18, 1
Prantzos, N., & Diehl, R. 1996, Phys. Rep., 267, 1
Rice, E. L., Prato, L., & McLean, I. S. 2006, ApJ, 647, 432
Robin, A. C., Reylé, C., Derrière, S., & Picaud, S. 2003, A&A, 409, 523
Roques, J. P., Schanne, S., von Kienlin, A., et al. 2003, A&A, 411, L91
Smith, D. M. 2003, ApJ, 589, L55
Strong, A. W., Bloemen, H., Diehl, R., Hermsen, W., & Schönfelder, V. 1999, Astrophys. Lett. Comm., 39, 209
Strong, A. W., Diehl, R., Halloin, H., et al. 2005, A&A, 444, 495
Taylor, J. H., & Cordes, J. M. 1993, ApJ, 411, 674
Verley, S., Combes, F., Verdes-Montenegro, L., Bergond, G., & Leon, S. 2007, A&A, 474, 43
Wang, W., Jiang, Z. J., Pun, C. S. J., & Cheng, K. S. 2005, MNRAS, 360, 646
Wang, W., Harris, M. J., Diehl, R., et al. 2007, A&A, 469, 1005
Weidenspointner, G., Skinner, G., Jean, P., et al. 2008, Nature, 451, 159
Wheelock, S., Chillemi, J., Gautier, N., et al. 1991, BAAS, 908
Woosley, S. E., & Heger, A. 2007, APS 2005 Bethe Prize Lectures, Phys. Rep., 442, 269